Effects of fluxon dynamics on higher harmonics of ac susceptibility in type-II superconductors

P. Fabbricatore, S. Farinon, G. Gemme, R. Musenich, R. Parodi, and B. Zhang
Istituto Nazionale di Fisica Nucleare, Sezione di Genova, via Dodecaneso 33, I-16146 Genova, Italy
(Received 25 February 1994)

Measurements of fundamental and higher harmonics of ac susceptibility of polycrystalline low-T_c and high-T_c superconductors show a failure of the critical-state model in describing the higher harmonics dependence on temperature at fixed dc and ac magnetic fields. The results of measurements at different frequencies suggest that an effect of the fluxon dynamics could take place. Indeed simple considerations lead to the conclusion that thermally activated flux flow, flux creep, and flux flow (FF) should have an important role in determining the higher harmonics of ac susceptibility. A simplified critical-state model, only including pinning and FF, seems to explain part of the experimental results.

I. INTRODUCTION

ac magnetic susceptibility is perhaps the most used experimental technique to study the electrical and magnetic properties of superconductors. The fundamental in-phase χ'' and out-of-phase χ' components are measured as reported in the complete review paper of Goldfarb.[1] Some authors[2,3] measure the wide band susceptibility, which also contains information about higher harmonics. In some cases[4–9] measurements of higher harmonics of the ac susceptibility are reported. The authors stress the agreement of results with predictions of the Bean or Kim-Anderson critical-state model.[10–12] We developed an experimental method,[13] which allows to measure at the same time the fundamental and the higher harmonics as a function of the temperature. In order to simplify the interpretation of the experimental results, the measurements, on a variety of type-II superconducting materials, were carried out at a fixed dc magnetic field much higher than the ac magnetic field. In this case the simple Bean model would describe the field penetration inside the sample. A further advantage of using this technique is that the field penetration is symmetric with respect to the external dc field, so that only odd harmonics are measured. The results show a disagreement with the critical-state model of the third and fifth harmonics, depending on the frequency of the ac field. This occurrence suggests the idea of a strong effect of the fluxon dynamics on the higher harmonics. In this paper, after a review of the expected behavior of the first three odd harmonics vs temperature according to the Bean model and Kim model, some experimental results are shown, followed by a discussion on the effects of fluxon dynamics.

II. HARMONICS OF AC SUSCEPTIBILITY VS TEMPERATURE

On applying an ac magnetic field $B(t)=B_0\cos(\omega t)$ to a superconducting sample and detecting the flux variations through two pickup coils, one of which is surrounding the sample, a signal proportional to the derivative of magnetization is obtained $u(t)=u_1(t)-u_2(t)\propto dM/dt$, where $u_1(t)$ is the signal in the pickup coil containing the sample and $u_2(t)$ the signal in the other one. The signal $u(t)$ can be developed in a Fourier series as

$$u(t)=\sum_{n=1}^{\infty}(a_n\cos n\omega t+b_n\sin n\omega t)\ . \tag{1}$$

The coefficients a_n and b_n are obtained as

$$a_n=\frac{2}{t_0}\int_0^{t_0}u(t)\cos(n\omega t)\,dt\ , \tag{2a}$$

$$b_n=\frac{2}{t_0}\int_0^{t_0}u(t)\sin(n\omega t)dt\ , \tag{2b}$$

where t_0 is the period of the oscillation. The ac susceptibility components usually measured are $\chi_1'=b_1/C$ and $\chi_1''=a_1/C$, where C is a factor depending on both frequency and experimental setup.

The coefficients a_n and b_n can be analytically calculated if the field penetrates a cylindrical sample according to the Bean model

$$B(r,t)=B(R,t)\pm\mu_0 J_c(r-R)\ , \tag{3}$$

where r is a position inside the sample, R is the sample radius, and J_c is the critical current density. The + sign means that fluxons are entering into the sample (increasing field); the − sign for fluxons leaving the sample (decreasing field). Setting

$$r^*=R-\frac{B_0}{\mu_0 J_c(T)}\ , \tag{4a}$$

the radius at which the field penetrates the sample, and

$$\theta=\arccos\left[1-\frac{2\mu_0 R J_c(T)}{B_0}\right], \tag{4b}$$

we obtain for the three odd coefficients, as function of the critical current density:

$$a_1=\begin{cases}\frac{2}{3}B_0\omega(r^*-R)(r^*+R)\ , & \text{if } J_c(T)\geq\frac{B_0}{\mu_0 R}\\ \frac{1}{6}B_0R^2\omega(\cos\theta-1)(\cos\theta+3)\ , & \text{if } J_c(T)\leq\frac{B_0}{\mu_0 R}\ ,\end{cases} \tag{5a}$$

$$b_1=\begin{cases}-\frac{\pi B_0}{16}\left[(r^*-R)^2+4(r^*+R)^2\right]\ , & \text{if } J_c(T)\geq\frac{B_0}{\mu_0 R}\\ -\frac{B_0\omega R^2}{12(\cos\theta-1)^2}(12\theta\cos^2\theta+3\theta-13\cos\theta\sin\theta-2\sin\theta\cos^3\theta)\ , & \text{if } J_c(T)\geq\frac{B_0}{\mu_0 R}\ ,\end{cases} \tag{5b}$$

$$a_3=\begin{cases}-\frac{2}{5}B_0\omega(r^*-R)(r^*+R)\ , & \text{if } J_c(T)\geq\frac{B_0}{\mu_0 R}\\ \frac{B_0\omega R^2}{30}(\cos\theta-1)(4\cos^3\theta+12\cos^2\theta+9\cos\theta-5)\ , & \text{if } J_c(T)\leq\frac{B_0}{\mu_0 R}\ ,\end{cases} \tag{5c}$$

$$b_3=\begin{cases}-\frac{\pi B_0\omega}{16}(r^*-R)^2\ , & \text{if } J_c(T)\geq\frac{B_0}{\mu_0 R}\\ \frac{B_0\omega R^2}{12(\cos\theta-1)^2}(-26\sin\theta\cos^3\theta+8\sin\theta\cos^5\theta-15\theta+33\cos\theta\sin\theta)\ , & \text{if } J_c(T)\leq\frac{B_0}{\mu_0 R}\ ,\end{cases} \tag{5d}$$

$$a_5=\begin{cases}-\frac{2}{21}B_0\omega(r^*-R)(r^*+R)\ , & \text{if } J_c(T)\geq\frac{B_0}{\mu_0 R}\\ \frac{B_0\omega R^2}{42}(\cos\theta-1)(8\cos^5\theta+24\cos^4\theta+20\cos^3\theta-4\cos^2\theta-13\cos\theta-7)\ , & \text{if } J_c(T)\leq\frac{B_0}{\mu_0 R}\ ,\end{cases} \tag{5e}$$

$$b_5=\begin{cases}0\ , & \text{if } J_c(T)\geq\frac{B_0}{\mu_0 R}\\ -\frac{4}{21}\frac{B_0\omega R^2}{(\cos\theta-1)^2}\cos\theta\sin^7\theta\ , & \text{if } J_c(T)\leq\frac{B_0}{\mu_0 R}\ .\end{cases} \tag{5f}$$

The higher harmonics of ac susceptibility can be calculated as function of the temperature if the $J_c(T)$ curve is known. Supposing the critical current density to be a function of temperature as

$$J_c=J_{c0}\left[1-\frac{T}{T_c}\right]^n\ , \tag{6}$$

we obtain a temperature behavior for the first three odd harmonics as shown in Fig. 1, where the components χ_n' and χ_n'' are shown as well as the module $\chi_n=c_n/C=(\sqrt{a_n^2+b_n^2})/C$, which is of interest for a later discussion.

Using the Kim model, the critical-state equation can be written as

$$\frac{\partial B}{\partial r}=\pm\mu_0 J_c^*\frac{\beta}{\beta+|B|}\ , \tag{7}$$

where J_c^* and β are pinning parameters. In this case the field penetration is much more complex than the simple result given by Eq. (3). Setting $\alpha=\mu_0 J_c^*\beta$, we obtain in the time interval $0<t<t_0/4$

$$B(r)=\begin{cases}0\ , & \text{if } 0\leq r\leq r_0\\ -\beta+\sqrt{\beta^2+B_0^2+2\beta B_0-2\alpha(R-r)}\ , & \text{if } r_0\leq r\leq r_1\\ -\beta+\sqrt{\beta^2+B_0^2\cos^2\omega t+2\beta B_0\cos\omega t+2\alpha(R-r)}\ , & \text{if } r_1\leq r\leq R\ ,\end{cases} \tag{8a}$$

where

$$r_0 = R - \frac{B_0(B_0+2\beta)}{2\alpha} ,$$

$$r_1 = R - \frac{B_0(1-\cos\omega t)(B_0(1+\cos\omega t)+2\beta)}{4\alpha} .$$

In the time interval $t_0/4 < t < t_0/2$

$$B(r) = \begin{cases} 0 , & \text{if } 0 \le r \le r_0 \\ -\beta + \sqrt{\beta^2 + B_0^2 + 2\beta B_0 - 2\alpha(R-r)} , & \text{if } r_0 \le r \le r_2 \\ -\beta + \sqrt{\beta^2 - B_0^2\cos^2\omega t + 2\beta B_0\cos\omega t + 2\alpha(R-r)} , & \text{if } r_2 \le r \le r_3 \\ \beta + \sqrt{\beta^2 + B_0^2\cos^2\omega t - 2\beta B_0\cos\omega t - 2\alpha(R-r)} , & \text{if } r_3 \le r \le R , \end{cases} \tag{8b}$$

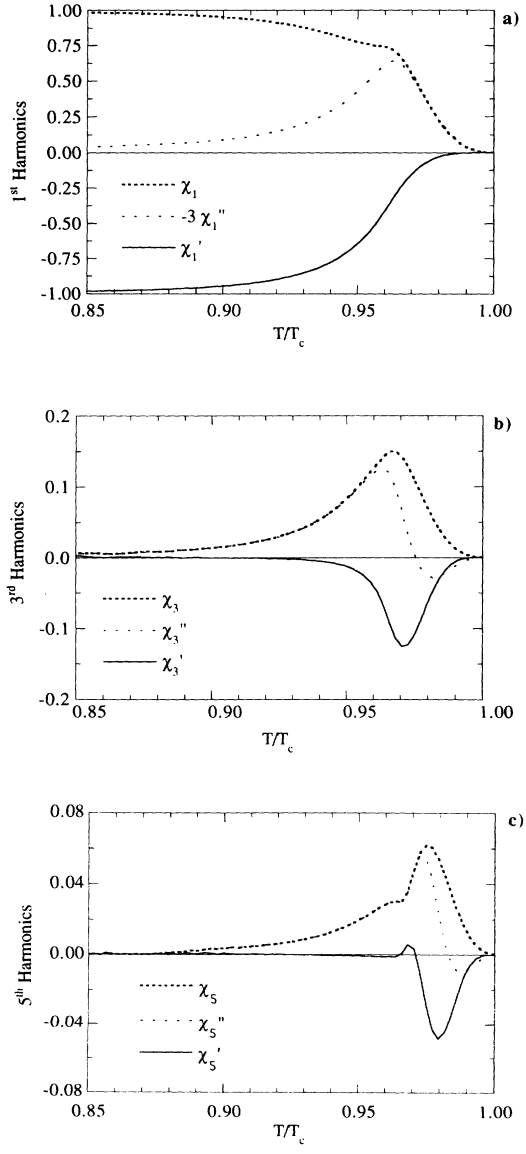

FIG. 1. Calculated odd harmonic components of ac susceptibility vs temperature according to the Bean model. (a) fundamental, (b) third harmonics, (c) fifth harmonics.

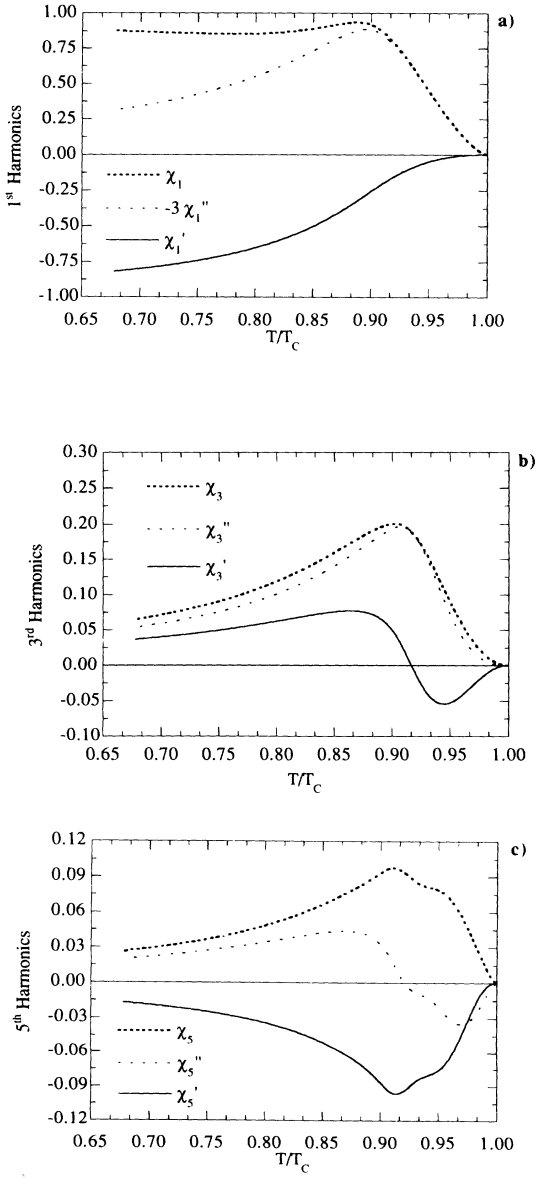

FIG. 2. Calculated odd harmonics using the Kim model. (a) fundamental, (b) third harmonics, (c) fifth harmonics.

where

$$r_2 = R - \frac{B_0^2(1+\cos^2\omega t)+2\beta B_0(1-\cos\omega t)}{4\alpha}$$

$$r_3 = R - \frac{B_0\cos\omega t(B_0\cos\omega t-2\beta)}{2\alpha} .$$

In the time interval $t_0/2 < t < t_0$ $B(r,t) = -B(r,t-t_0/2)$. In this case the integration of Eq. (2) can be carried out numerically. The results for the harmonic coefficients and the modules are shown in Fig. 2.

III. EXPERIMENTAL RESULTS

In order to measure the harmonic coefficients as function of the temperature, we used two experimental setups. In the basic setup[13] [Fig. 3(a)] the signal $u(t)$ is sent to a signal analyzer, which performs the fast Fourier transforms and measures the first 20 in-phase and out-of-phase components. In a further setup [Fig. 3(b)] used for comparison, the signal $u(t)$ is sent to a lock-in amplifier, having as reference a signal oscillating at a frequency $n\omega$. In this case only the nth harmonics are measured. The measurements were performed on different samples, described in Table I.

The results were very similar for all the samples. Figure 4 shows the first three odd harmonics components vs temperature as measured for the sample NT1, placed in a dc magnetic field of 1 T and an ac magnetic field of 5-G peak value. As before remarked, a dc magnetic field $B_{dc} = 1T \gg B_0$ was applied in order to have both a field penetration as predicted by the Bean model and the presence of only the odd harmonics. The measurements were carried out at different frequencies, in the figure the results obtained in the range (0.7–7.7 Hz) are shown. At increasing frequencies the following features were observed:

(1) The first harmonic components have identical shape. A light shift towards higher temperatures takes place. This is a typical behavior of the fundamental component of the ac susceptibility vs temperature.[14]

(2) The third harmonic components approximate the Bean model [Fig. 1(b)] only at lower frequencies. At 7.7 Hz the curves are completely reversed with respect to the expected ones.

(3) The fifth harmonic components approximate the Bean model at higher frequencies (the out-of-phase component better than the in-phase component).

Other measurements performed in the frequency range (7.7–100 Hz) show few changes with respect to the 7.7-Hz measurements. Similar behavior was observed on the NTTZ1 and BISCCO1 samples. Figure 5 shows some results of the third harmonics for these samples. For the NbTi samples the higher harmonic components were also measured at fixed frequency (0.7 Hz) and different ac magnetic field peak amplitudes. In this case no anomalous behavior was observed.

The experimental results show that the frequency of the ac magnetic field strongly affects the higher harmonics vs temperature curves. This occurrence suggests that the fluxon dynamics should be included in the critical-state model. In the next section we will try to introduce some dynamic mechanisms like flux flow. Before concluding this section we stress three points:

(1) Some authors[4–6] measured the module of higher harmonics $c_n = \sqrt{a_n^2+b_n^2}$. In these cases the information coming from the sign of each component are fully lost, so that the experimental results seem to agree with the Bean model. As an example Fig. 6 shows $\chi_3(T) = c_3(T)/C$, i.e., the module of the third harmonic, obtained from the components as given in Figs. 4(c) and 4(d). Though a light frequency dependence is observed, the Bean model seems to be confirmed [see Fig. 1(b)].

(2) We were able to observe the deviations from the Bean model because, using the network analyzer, we measured the harmonic components vs the temperature at the same time. This technique allows to detect immediately anomalous behavior. As an example, the Bean model predicts that the in-phase harmonics χ_1'' and χ_3''

TABLE I. Characteristics of the used samples.

Sample	Composition	Structure	T_{c0} (K)	Shape and dimensions (mm)
NT1	NbTi alloy	bcc polycrystalline	9.29	Cylindrical diameter 1 length 10
NT2	NbTi alloy	bcc polycrystalline	9.31	Parallelepiped 1×2×10
NTTZ1	$Nb_{0.4}Ti_{0.45}Ta_{0.075}Zr_{0.075}$	bcc polycrystalline	9.16	Tape 0.1×2×10
BISCCO1	$Bi_2Sr_2CaCu_2O_{8-x}$ melted	Orthorhombic polycrystalline	86.7	Cylindrical diameter 0.6 length 10
BISCCO2	$Bi_2Sr_2CaCu_2O_{8-x}$ melted	Orthorhombic polycrystalline	86.4	Parallelepiped 0.5×1×10

have opposite sign. We observed on the contrary the same sign of these harmonic components down to very low frequencies, as discussed before. On performing measurements of a single harmonic, the anomalous behavior could not be observed due to the characteristics of the experimental setup.

A central experimental problem is the phase of the signals at the pickup coils $u_1(t)$ and $u_2(t)$, with respect to the oscillating field. For a correct measurement this phase should be adjusted at 90° when the sample is in the normal state. Using the setup shown in Fig. 3(a), the phase adjustment is made monitoring the signal $u_2(t)$ in the pickup coil not containing the sample. The phase is regulated so that the network analyzer measures the maximum value of $u_2(t)$ out-of-phase (90°) and zero value in-phase.

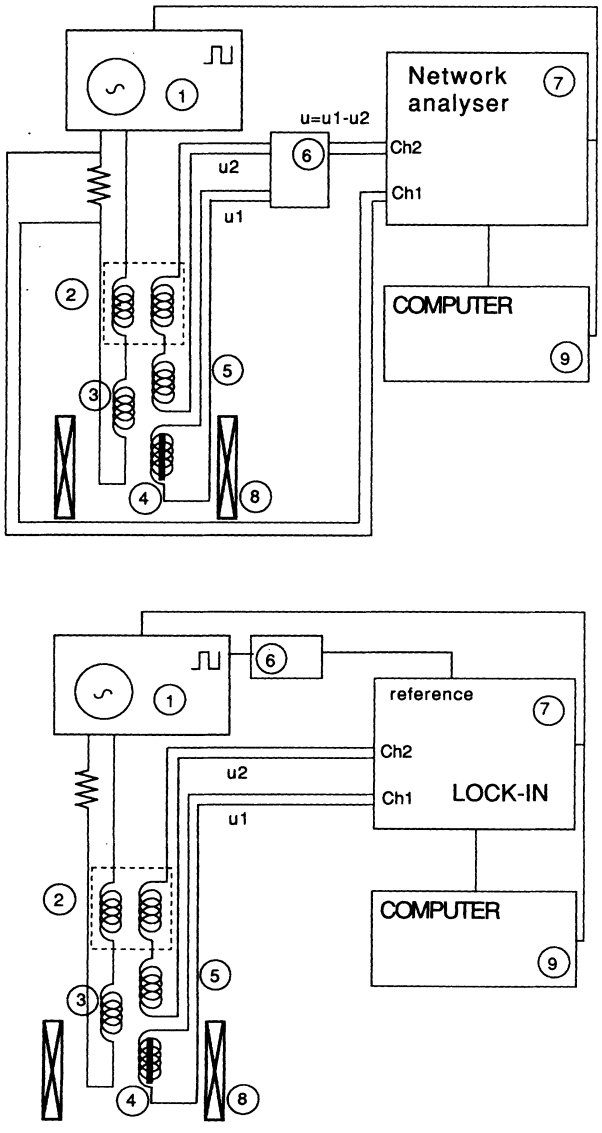

FIG. 3. Experimental setups. (a) multiple harmonics measurement: 1, wave generator; 2, flux transformer; 3, primary coil; 4, pickup coil containing the sample; 5, balancing pickup coil; 6, signal selector; 7, network analyzer; 8, dc magnet; 9, controller. (b) signal harmonic measurement. The components differing from (a) are 6, band-pass filter; 7, lock-in amplifier.

The measurement of the nth single harmonic is made by using, as reference for the lock-in amplifier, a signal oscillating at the frequency $n\omega$ as shown in Fig. 3(b). In this case the phase procedure depends on the harmonics. For the fundamental one the phase is regulated with the method before described, i.e., $u_2(t)$ must be maximum, out-of-phase, measured using the lock-in. For higher harmonics the phase procedure is different. Since no higher harmonics can exist when the sample is in the normal state, the field must oscillate according to a square wave for the phase adjustment (not for the measurement). In this way we can select the higher harmonics of $u_2(t)$ [let us call $u_2^n(t)$] to control the phase. Using this method for harmonics measurement, the phase is different for each harmonic so that the correlation of results of different harmonics can be ambiguous. Furthermore, in the range of frequencies normally used (10–100 Hz or more), the third harmonic components are exactly reversed with respect to the Bean model, so that a not identified phase error can lead to wrong conclusions. This is the main reason for using the multiple harmonics measurements with the network analyzer.

(3) The harmonics vs temperature curves, shown in Figs. 1 and 2, were calculated for cylindrical geometry. Similar curves are obtained for infinite slab. Only NT1, NTTZ1, and BISCCO1 samples correspond to these geometric conditions. Indeed the flux penetration could be not uniform unless dependent upon the micromorphology of the materials.[15] In this case the flux penetration would be so complex that no trivial corrections to the harmonic coefficients, as expressed by Eq. (5), are required. Though this effect does not account for the strong frequency dependence of the higher harmonics vs temperature curves, it remains an open question for further developments.

IV. EFFECTS OF FLUXON DYNAMICS

We restricted our attention to the dynamic effects, which causes the generation of an electric field. The reason for this is that the appearance of fundamental and higher harmonics of susceptibility can be related to an irreversible magnetic behavior. In fact the measurements clearly show that, on cooling the sample, the variation of the in-phase harmonic χ_1'', which has the meaning of dissipated energy related to a magnetic irreversibility, is the first evidence of a superconducting behavior. This means that the higher harmonics are different from zero in a temperature range dominated by irreversible phenomena. Fluxon movements also can occur at temperatures higher than the χ_1'' onset without energy dissipation. These dynamic effects, related to the melting of the Abrikosov lattice,[16,17] do not cause irreversibility and cannot have effect on fundamental and higher harmonics.

Figure 7 shows the E-J characteristics of a superconductor at different temperatures. Three different regimes exist with three different resistivity behaviors:[18]

$$\text{flux flow}\ , \quad \rho_{FF} \sim \rho_n \frac{B}{B_{c2}}\ , \tag{9a}$$

thermally activated flux flow , $\rho_{\mathrm{TAFF}} \sim \rho_n \frac{B}{B_{c2}} e^{-U/kT}$, (9b)

flux creep , $\rho_{\mathrm{FC}} \propto e^{(J/J_c)(U/kT)}$, (9c)

where U is the pinning energy. For low-T_c typical values are $\rho_{\mathrm{FF}} \sim 10^{-8}$ Ωm; $\rho_{\mathrm{FC}} \sim 10^{-13}$ Ωm; $\rho_{\mathrm{TAFF}} \sim 10^{-17}$ Ωm.

On performing an ac magnetic measurement, we impose an oscillating electric field of maximum amplitude $E = B_0 \omega R$. From Fig. 7 we see that moving from higher to lower temperatures, i.e., from lower to higher critical current densities, the fluxons can experience all the three dynamic regimes, starting from the FF very close to the normal to superconducting transition. Depending on the amplitude of the electric field we can have FF and then FC (high amplitude—line *a* in Fig. 7) or FF and TAFF (low amplitudes—line *b*).

We can understand which is the dominant dynamic regime at some temperatures through the analysis of the in-phase component χ_1'' as function of temperature and frequency as shown in Fig. 4(b). From the values of frequency and of χ_1'' is possible to calculate the resistivity in the temperature region from the peak of χ_1'' to the critical temperature.

Let us define the resistivity through the relation $\rho \sim \Delta E / \Delta J$, the value of the electrical field being the maximum external one: $E = B_0 \omega R$, so that, on performing measurements at different frequencies, we obtain curves with different electrical fields. The critical current density can be calculated applying the Bean model:

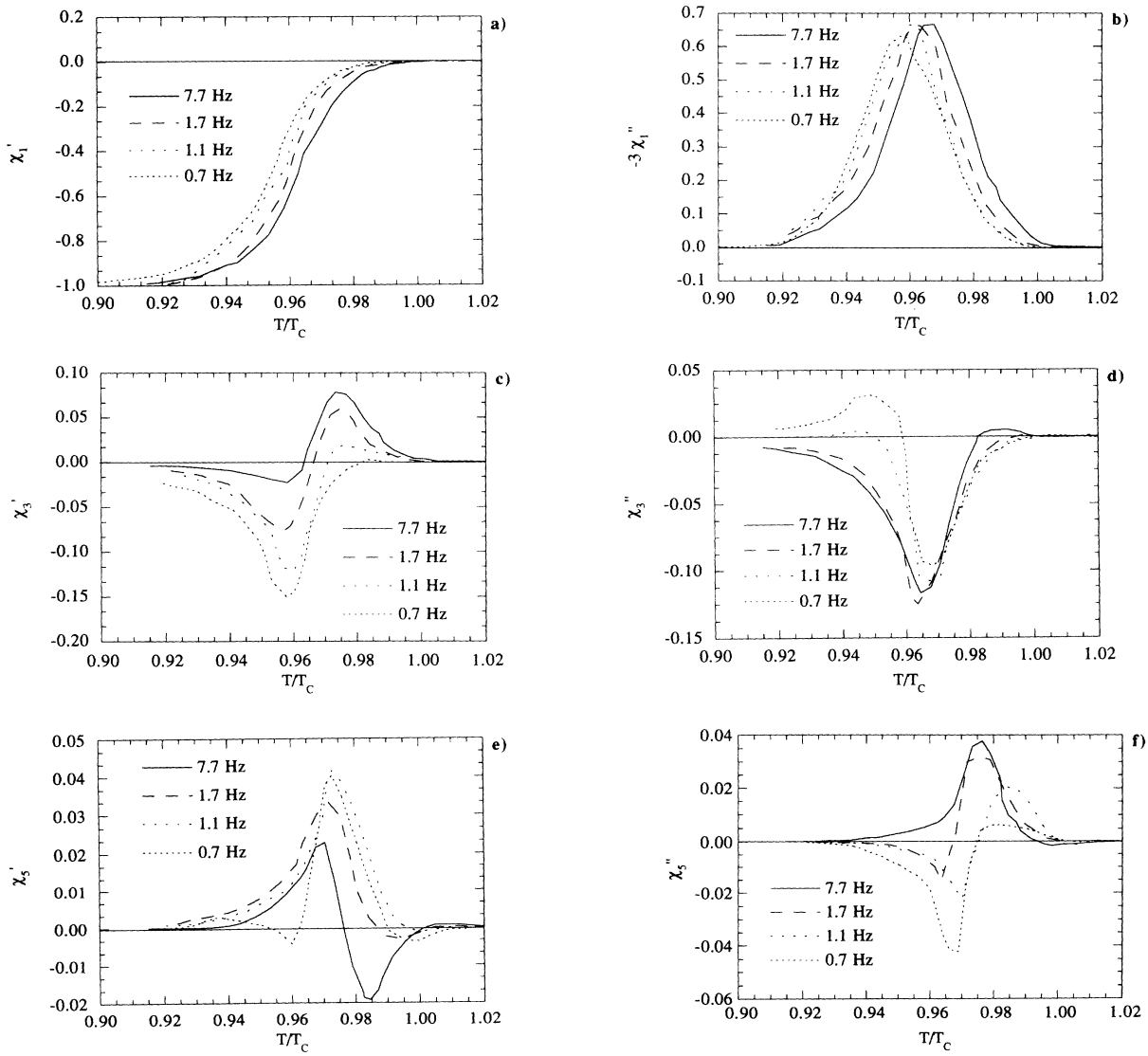

FIG. 4. Measured odd harmonics in the frequency range 0.7–7.7 Hz on the sample NT1 ($T_c = 8.8$ K at $B = 1$ T). (a) fundamental out-of-phase; (b) fundamental in-phase; (c) third harmonic out-of-phase; (d) third harmonic in-phase; (e) fifth harmonic out-of-phase; (f) fifth harmonic in-phase. The critical temperature is defined as the onset of χ_1''.

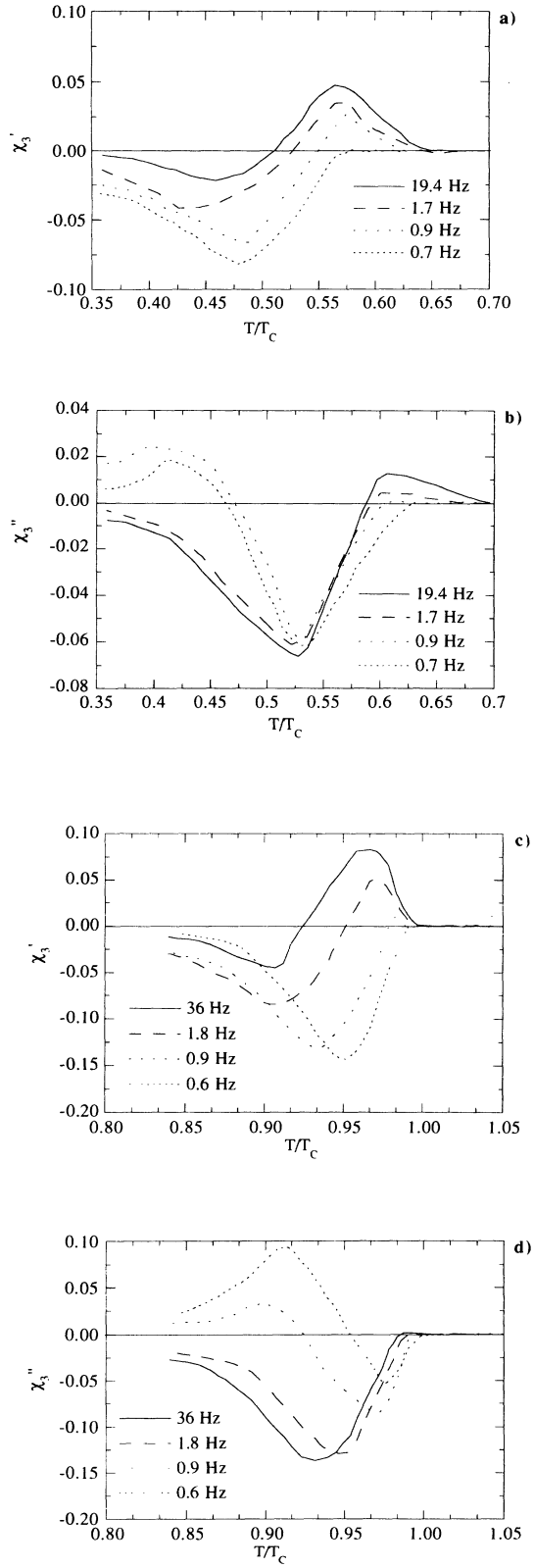

FIG. 5. Third harmonics of the BISCCO1 sample (a) in-phase; (b) out-of-phase with $T_c(B=1\text{ T}) = 85$ K, and for the NTTZ1 sample (c) in-phase; (d) out-of-phase with $T_c(B=1\text{ T}) = 8.55$ K. To be noted that in the Bi-based sample the onset of harmonics is the irreversibility temperature $T_{irr}=0.7T_c=59.5$ K.

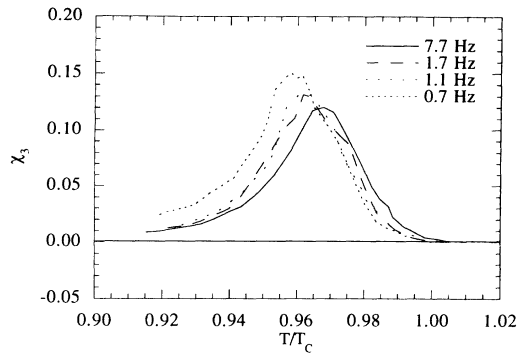

FIG. 6. Third harmonic $\chi_3(T)=c_3(T)/C$ of NT1 sample in the frequency range 0.7–7.7 Hz.

$$\chi_1''=-\frac{2}{3\pi}\left[\frac{\mu_0 R J_c}{B_0}\right]\left[2-\frac{\mu_0 R J_c}{B_0}\right]. \tag{10}$$

At a fixed temperature we have different values of χ_1'' depending on the frequency. Calculating E and J_c for each χ_1'' value, we can obtain the resistivity. For the NbTi sample in the temperature rangle 8.4–8.6 K we obtain $\rho\approx 10^{-9}$ Ωm. This value of resistivity is intermediate between FC and FF, closer to FF. Since the FF seems to dominate in proximity to the transition, we can try to include this effect in the critical-state model and to calculate the effects on the first three odd harmonics.

A. Diffusion equation

For simplicity we will study the problem related to a superconducting slab of thickness $2x_0$, with the magnetic field applied parallel to the slab. It is well known[19] that the viscous force can be represented as a term depending on the fluxon velocity v and the viscosity η, $F_v=\eta/\Phi_0 v=B_c 2/\rho n v$:

$$\frac{1}{\mu_0}\frac{\partial B}{\partial x}=\pm J_c\pm\frac{B_{c2}}{\rho_n}v\ . \tag{11}$$

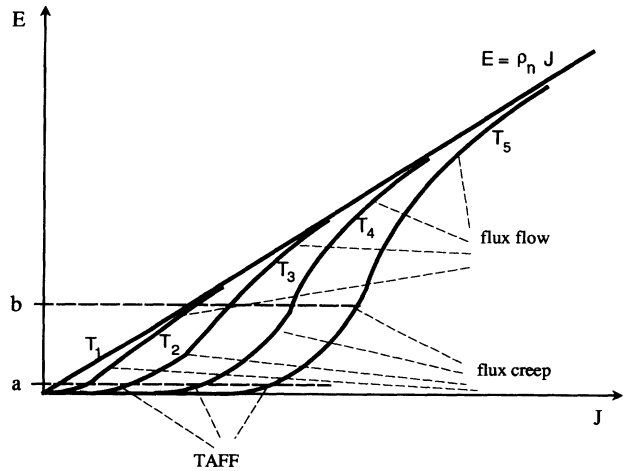

FIG. 7. E-J characteristics of a pinned superconductor at decreasing temperatures $T_1>T_2>T_3>\ldots$, with evidence of the three dynamic regimes: TAFF, FC, and FF.

B_{c2} is the upper critical field and ρ_n is the normal-state resistivity.

Since $E=vB$ and $\partial E/\partial x=\partial B/\partial t$, we have

$$\pm B\frac{\partial^2 B}{\partial x^2}\pm\left[\frac{\partial B}{\partial x}\right]^2-\mu_0 J_c\frac{\partial B}{\partial x}=\frac{\mu_0 B_{c2}}{\rho_n}\frac{\partial B}{\partial t}\ . \tag{12}$$

This equation cannot be solved analytically, but interesting information comes from some approximations. In fact supposing the viscous force to be much higher than the pinning force,[19] Eq. (11) can be written as

$$\frac{\partial}{\partial x}\left[B\frac{\partial B}{\partial x}\right]=\frac{\mu_0 B_{c2}}{\rho_n}\frac{\partial B}{\partial t}\ . \tag{13}$$

This is a nonlinear diffusion equation similar to the equations obtained for the TAFF (Ref. 20) or for the FC.[21] Using these equations a numerical solution could be found for the field penetration and then for ac susceptibility. Nevertheless a simple analysis shows that this approach does not explain the higher harmonics behavior in the case of a small ac field superimposed to a constant dc field.

Figure 8 shows that, using the Bean model, in the region from x_p, where the ac field penetrates, to the surface x_0, the magnetic field can be written as the sum of a constant field (the external dc magnetic field $B_{\mathrm{dc\ ext}}$) plus the ac field B_{ac}: $B=B_{\mathrm{dc\ ext}}+B_{\mathrm{ac}}(x,t)$. In the region $0<x<x_p$ the field is given by $B=B_{\mathrm{dc}}(x)+B_0$. Since the latter region gives no contribution to the ac susceptibility, we can write $\partial B/\partial x=\partial B_{\mathrm{ac}}/\partial x$. Furthermore since the dc field is not time dependent, we have $\partial B/\partial t=\partial B_{\mathrm{ac}}/\partial t$, so that Eq. (13) can be rewritten as

$$\frac{\mu_0 B_{c2}}{\rho_n}\frac{\partial B_{\mathrm{ac}}}{\partial t}-B_{\mathrm{dc}}\frac{\partial^2 B_{\mathrm{ac}}}{\partial x^2}=\frac{\partial}{\partial x}\left[B_{\mathrm{ac}}\frac{\partial B_{\mathrm{ac}}}{\partial x}\right]\ . \tag{14}$$

In our case $B_{\mathrm{ac}}\ll B_{\mathrm{dc}}$ so that the right side of Eq. (14) can be set to zero, obtaining a linear diffusion equation. Solving this equation with the boundary conditions $B_{\mathrm{ac}}(x_0,t)=B_0\cos(\omega t)$ and $B_{\mathrm{ac}}(0,t)=0$, i.e., at the complete field penetration, we obtain

$$B_{\mathrm{ac}}(x,t)=A_1(x)\cos\omega t+A_2(x)\sin\omega t\ . \tag{15}$$

The meaning of Eq. (15) is that the internal field can be completely described in terms of the fundamental frequency, so that no higher harmonics could be expected for the ac susceptibility. The higher harmonics come from the irreversibility due to the pinning force. The theories, which analyze a single dynamic regime neglecting the pinning term, result to be incomplete.

We stress again that this result is valid only in the approximation $B_{\mathrm{ac}}\ll B_{\mathrm{dc}}$. It could be interesting to show that for a dc field value approaching to zero, we have instead a strong generation of higher harmonics. This can be seen solving Eq. (14) for half the plane, defined by $x>0$ with the boundary condition $B_{\mathrm{ac}}(x=0,t)=B_0\cos\omega t$. The solution can be written as

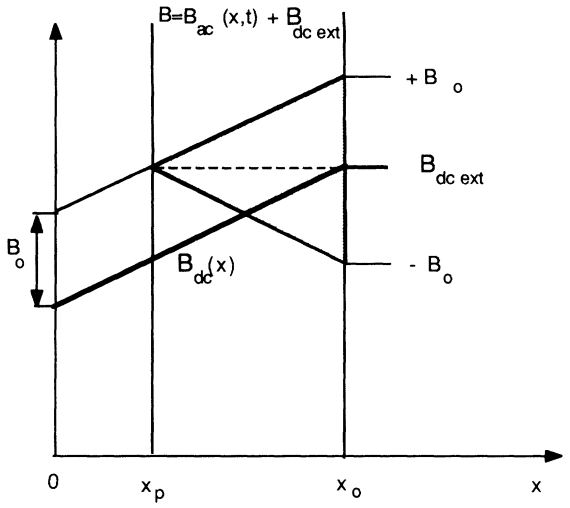

FIG. 8. Flux penetration in a slab using the Bean model. The shadowed area represents the ac magnetic flux penetration. The thick line is the dc field presentation.

$$B_{\mathrm{ac}}(x,t)=\sum_1^\infty \beta_n(x,t) \tag{16}$$

where β_0 is the solution of the linear diffusion equation obtained setting to zero the left side of Eq. (14),

$$\beta_0(x,t)=B_0\exp\left[-\sqrt{\omega\rho_n B_{\mathrm{dc}}/2\mu_0 B_{c2}}\,x\right]\times\cos\left(-\sqrt{\omega\rho_n B_{\mathrm{dc}}/2\mu_0 B_{c2}}\,x+\omega t\right) \tag{17}$$

and β_n are the higher-order approximations defined by the recurrent equation

$$\frac{\mu_0 B_{c2}}{\rho_n}\frac{\partial\beta_n}{\partial t}-B_{\mathrm{dc}}\frac{\partial^2\beta_n}{\partial x^2}=\sum_{\nu=0}^{n-1}\frac{\partial}{\partial x}\left[\beta_\nu\frac{\partial\beta_{n-\nu-1}}{\partial x}\right]\ . \tag{18}$$

Each β_n can be obtained through

$$\beta_n(x,t)=\int dy\ G(x,y,t)\sum_{u=0}^{n-1}\frac{\partial}{\partial x}\left[\beta_u\frac{\partial\beta_{n-u-1}}{\partial x}\right]_y\ , \tag{19}$$

where $G(x,y,t)$ is the Green function defined by the relation

$$G(x,y,t)=g(x,y)e^{i\omega t}\ , \tag{20}$$

$$\frac{\mu_0 B_{c2}}{\rho_n}\frac{\partial g}{\partial t}-B_{\mathrm{dc}}\frac{\partial^2 g}{\partial x^2}=\delta(x-y)\ . \tag{21}$$

It is found that $G(x,y,t)$ has the form

$$G(x,y,t)=\frac{\exp\left[-(1+i)\sqrt{\omega\rho_n B_{\mathrm{dc}}/2\mu_0 B_{c2}}\,|x-y|\right]-\exp\left[-(1+i)\sqrt{\omega\rho_n B_{\mathrm{dc}}/2\mu_0 B_{c2}}\,|x+y|\right]}{(i+1)\sqrt{2\omega\mu_0 B_{c2}/\rho_n B_{\mathrm{dc}}}}e^{i\omega t}\ . \tag{22}$$

Replacing $G(x,y,t)$ in Eq. (19), we can see that the higher-order components generate higher harmonics, i.e., $\beta_n(x,t) \propto \cos(n+1)\omega t$ and that these components scale as

$$\frac{\beta_n}{\beta_{n-1}} \propto \frac{B_0}{B_{dc}} . \tag{23}$$

Equation (23) shows that for values of the ac field comparable with the dc field value, we can have significant higher harmonics generation. In our case the ratio $B_0/B_{dc}=10^{-3}$, so that it is confirmed the previous result, expressed by Eq. (15).

B. Constant fluxon velocity approximation

More information comes from an approximation of Eq. (12), which holds the pinning term. Supposing that the fluxon velocity is constant inside the sample, i.e., $\partial v/\partial x \sim 0$, it results $v=\partial B/\partial t/\partial B/\partial x$. Replacing the fluxon velocity in Eq. (11) and supposing to be in proximity to the normal to the superconducting transition, so that the field inside the sample is very close to the external magnetic field, Eq. (12) can be rewritten as

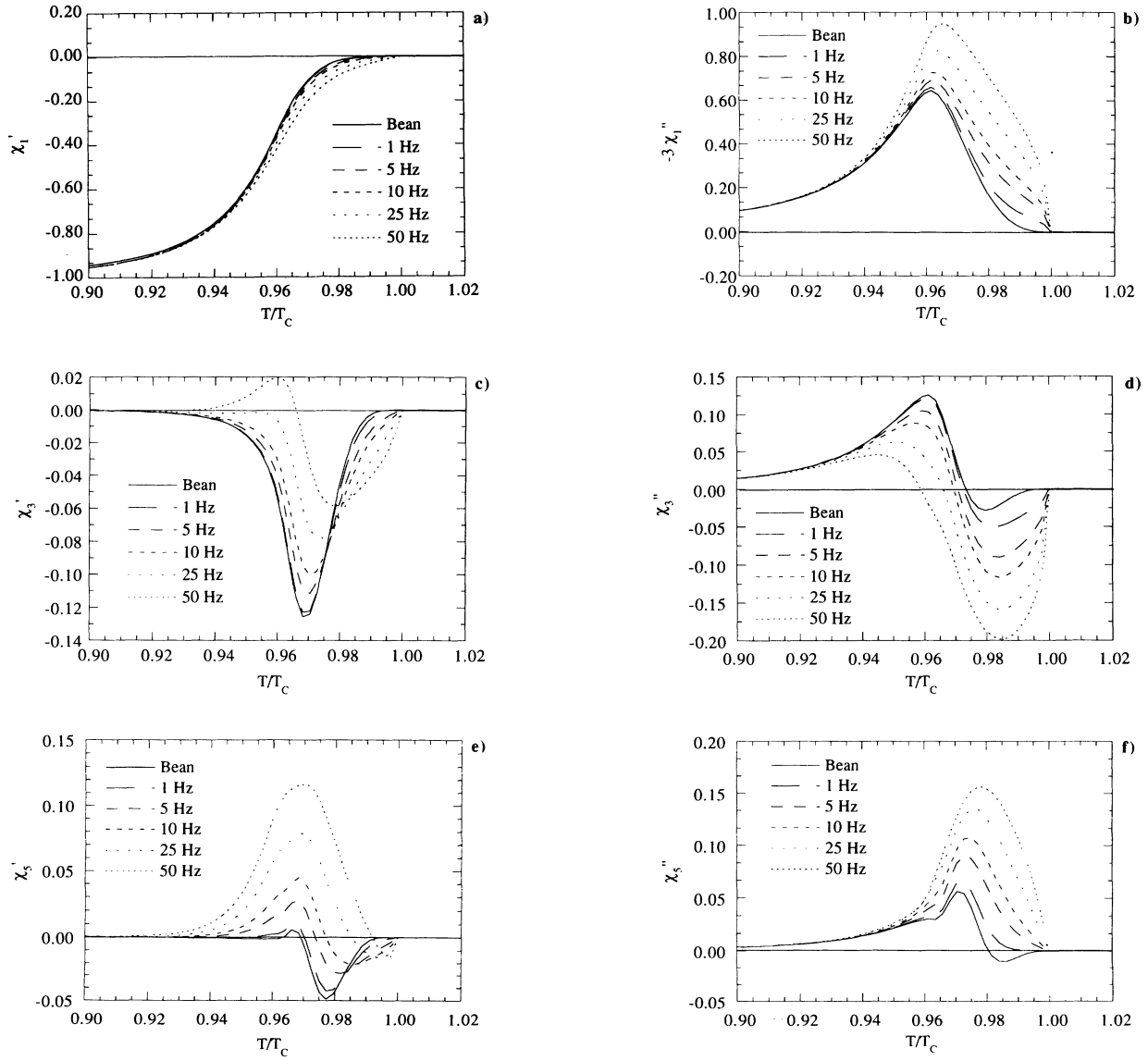

FIG. 9. Calculated harmonics for the NT1 sample using the constant fluxon velocity approximation. (a) fundamental out-of-phase; (b) fundamental in-phase; (c) third harmonic out-of-phase; (d) third harmonic in-phase; (e) fifth harmonic out-of-phase; (f) fifth harmonic in-phase.

$$\pm\left[\frac{\partial B}{\partial x}\right]^2-\mu_0 J_c\frac{\partial B}{\partial x}=-\frac{\mu_0\omega B_{c2}B_0\sin\omega t}{\rho_n}. \tag{24}$$

Solving, we obtain

$$B(x,t)=B_{\rm dc}+B_0\cos\omega t\mp\tfrac{1}{2}\mu_0 J_c\left[1+\left[1+\frac{4\omega B_{c2}B_0|\sin\omega t|}{\rho_n\mu_0 J_c^2}\right]^{1/2}\right](R-x)\ . \tag{25}$$

Equation (25) means that the ac field shielding depends on the ac field rate. At times $t=0$ and $t=t_0/2$ the field rate is zero so that the Bean model is valid. At times $t=t_0/4$ and $t=3t_0/4$ the field rate is maximum and equal to ωB_0, so that the shielding currents assume the maximum value. The harmonic components were calculated at frequencies 1, 5, 10, 25, and 50 Hz for a NbTi sample with the following characteristics: $B_{c20}=14$ T, $B_{\rm dc}=1$ T, $B_0=5$ G, $R=0.5$ mm and $\rho_n=10^{-7}$ Ωm. The critical current density was assumed to be given by Eq. (6) with $n=3$ and $J_{c0}=10^{11}$ A/m^2. The results are shown in Fig. 9. The first harmonic component χ_1' is weakly affected by the frequency of the ac field. The component χ_1'' assumes higher values at increasing frequencies, without changing its shape. The third harmonic components instead dramatically change moving from low to high frequencies. At 50 Hz the component χ_3'' has opposite sign with respect to its values at 1 Hz. The component χ_3' is also changing from negative to positive values. This behavior of calculated first and third harmonics seems to confirm the measurements. Unfortunately the fifth harmonics are not well described by the model, specially the in-phase component.

V. CONCLUSIONS

The critical-state model does not appear to account for the higher harmonics of ac susceptibility. Measurements on several type-II polycrystalline superconducting samples show a strong frequency dependence of the higher harmonics vs temperature. This occurrence led us to suppose some effects of the fluxon dynamics. We restricted our attention to FF, FC, and TAFF because we interpreted the nonzero values of the real part of ac susceptibility χ_1'' as indication of dissipated energy and then of an irreversible behavior. Time-dependent effects related to the melting of Abrikosov lattice were not considered. The inclusion of the flux flow in the critical-state equation led to a nonlinear diffusion equation. This equation was studied in the limit of the viscous force much higher than the pinning force. In the case of a small ac field superimposed to a constant dc field, no harmonic generation results. Since equations of the same kind can be written also for TAFF and FC, we drew the general conclusion that an approach to the fluxon dynamics, which is restricted to a single dynamic regime and neglects the pinning force, cannot account for higher harmonics. A simpler model, which considers the fluxon velocity constant inside the sample, seems to be in agreement with the experimental results of the third harmonics. The behavior of the fifth harmonics vs temperature is not explained in this framework.

ACKNOWLEDGMENTS

The authors express their thanks to Professor C. M. Becchi for the helpful discussions about the magnetic-field diffusion equations. Thanks are also due to Professor P. Ottonello for his suggestions in higher harmonics measurements.

[1]R. B. Goldfarb, M. Lelental, and C. A. Thompson, in *Magnetic Susceptibility of Superconductors and Other Spin Systems,* edited by R. A. Hein, T. L. Francavilla, and D. H. Liebenberg (Plenum, New York, 1991), p. 49.

[2]F. Gömöry, in *Magnetic Susceptibility of Superconductors and Other Spin Systems* (Ref. 1), p. 289.

[3]P. Fabbricatore, U. Gambardella, F. Gömöry, R. Musenich, M. Occhetto, R. Parodi, and P. Pompa, Rev. Sci. Instrum. **62**, 1796 (1991).

[4]T. Ishida and H. Mazaki, J. Appl. Phys. **52**, 6798 (1981).

[5]A. Shaulov and D. Dorman, Appl. Phys. Lett. **53**, 2680 (1988).

[6]L. Ji, R. H. Sohn, G. C. Spalding, C. J. Lobb, and M. Tinkham, Phys. Rev. B **40**, 10 936 (1989).

[7]T. Ishida and R. B. Goldfarb, Phys. Rev. B **41**, 8937 (1990).

[8]H. Mazaki, K. Yamamoto, and H. Yasouka, in *Magnetic Susceptibility of Superconductors and Other Spin Systems* (Ref. 1), p. 333.

[9]F. Weiss, J. Fick, J. Hudner, E. Mossang, Phan Quôc Phô, O. Thomas, and J. P. Sénateur, Cryogenics **33**, 497 (1993).

[10]C. P. Bean, Rev. Mod. Phys. **36**, 31 (1964).

[11]Y. B. Kim, C. F. Hempstead, and A. R. Strnad, Phys. Rev. **129**, 528 (1963).

[12]P. W. Anderson and Y. B. Kim, Rev. Mod. Phys. **36**, 39 (1964).

[13]P. Fabbricatore, S. Farinon, G. Gemme, R. Musenich, R. Parodi, and B. Zhang, Cryogenics **33**, 1170 (1993).

[14]A. P. Malozemoff, T. K. Worthington, Y. Yeshrun, F. Holtzberg, and P. H. Kes, Phys. Rev. B **38**, 7203 (1988).

[15]C. A. Durán, P. L. Gammel, R. Wolfe, V. J. Fratello, D. J. Bishop, J. P. Rice, and D. M. Ginsberg, Nature (London) **357**, 474 (1992).

[16]E. H. Brandt, Physica B **169**, 91 (1991).

[17]S. Sengupta, C. Dasgupta, H. R. Krishnamurty, G. I. Menom, and T. V. Ramakrishnam, Phys. Rev. Lett. **67**, 3444 (1991).
[18]E. H. Brandt, J. Supercond. **6**, 201 (1993).
[19]S. Takács, and F. Gömöry, Cryogenics **33**, 133 (1993).
[20]P. H. Kes, J. Aarts, J. van der Beek, and J. A. Mydosh, Supercond. Sci. Technol. **1**, 242 (1989).
[21]V. Calzona, M. R. Cimberle, C. Ferdeghini, G. Grasso, A. Iorio, F. Licci, M. Putti, C. Rizzuto, and A. S. Siri, Supercond. Sci. Technol. **6**, 46 (1993).

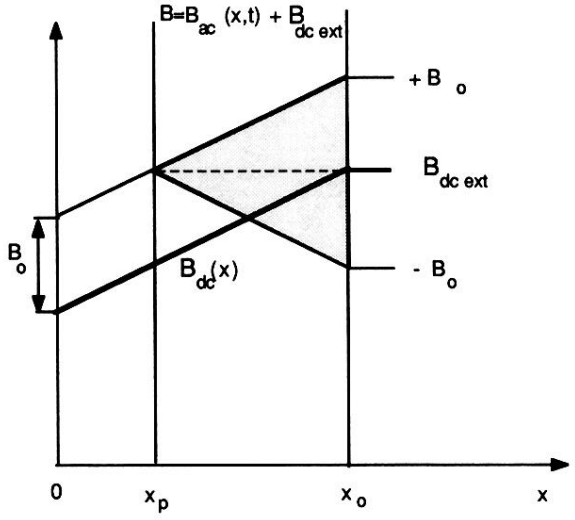

FIG. 8. Flux penetration in a slab using the Bean model. The shadowed area represents the ac magnetic flux penetration. The thick line is the dc field presentation.